Geomorphology 119 (2010) 74–87

Contents lists available at ScienceDirect

Geomorphology

journal homepage: www.elsevier.com/locate/geomorph

Active tectonics in the Sierra Nevada (Betic Cordillera, SE Spain): Insights from geomorphic indexes and drainage pattern analysis

José Vicente Pérez-Peña [a,*], Antonio Azor [a], José Miguel Azañón [a,b], Edward A. Keller [c]

[a] Departamento de Geodinámica, Universidad de Granada, Campus de Fuentenueva s/n, 18071 Granada, Spain
[b] Instituto Andaluz de Ciencias de la Tierra – Consejo Superior de Investigaciones Científicas (UGR-CSIC), Spain
[c] Department of Geological Sciences, University of California at Santa Barbara, CA 93106, USA

ARTICLE INFO

Article history:
Received 25 September 2009
Received in revised form 20 February 2010
Accepted 27 February 2010
Available online 8 March 2010

Keywords:
Tectonic geomorphology
Mountain fronts
Drainage pattern
Geomorphic indexes
Active folding and faulting
DEM

ABSTRACT

The Sierra Nevada of the central Betic Cordillera is a 3000 m-high mountain range surrounded by Neogene–Quaternary sedimentary basins, having been uplifted since Late Miocene times. The southern and western mountain fronts of the Sierra Nevada are fault-bounded, while the northern one is an unconformity between the Neogene–Quaternary sediments of the Guadix–Baza basin and the metamorphic rocks of the Nevado–Filabride complex. We have carried out a geomorphic study by examining drainage patterns and characteristics of mountain fronts in order to reveal areal variations and styles of rock uplift. Mountain front sinuosity (S_{mf}), area–altitude relations (hypsometric curves), and valley floor entrenchment differ significantly between the northern, western, and southern mountain fronts. The lack of important faults along the northern Sierra Nevada mountain front, together with the elevated topographic position of the Guadix–Baza basin (average altitude is around 1100 m), points to similar uplift of both geomorphic units (sierra and basin) in a single large-scale crustal block. The asymmetry factors show systematic asymmetries at both sides of the Lanjarón River, probably due to the presence of an active NNE–SSW oriented antiform in the western Sierra Nevada. Finally, river profiles indicate maximal river entrenchment in the western part of the Sierra Nevada, probably related to the uplift of the footwall of the Padul–Nigüelas fault-system. Therefore, our geomorphic analysis suggests that the western part of the Sierra Nevada is tectonically active by means of a combination of normal faults along the mountain front and NNE–SSW oriented active folds, which, in turn, likely have a gravitational origin related to the exhumation of the footwall of the normal fault-system.

1. Introduction

Active tectonics is one of the fastest growing disciplines in Earth Sciences due to the recent development of new geochronological and geodetic tools which facilitate the acquisition of accurate rates (uplift rates, incision rates, erosion rates, slip rates on faults, etc.) at variable (10^3–10^6 years) time-scales (e.g., Schumm et al., 2000; Burbank and Anderson, 2001; Keller and Pinter, 2002; Bull, 2007, 2009a,b). Furthermore, this discipline is becoming important because the results of regional studies on active tectonics are important for evaluating natural hazards, as well as for land use planning and management in populated areas (e.g., Cloetingh and Cornu, 2005). Apart from its social and economic interest, studies of active tectonics follow a multi-disciplinary approach, integrating data from structural geology, geomorphology, stratigraphy, geochronology, seismology, and geodesy.

In mountain ranges, recent and active tectonics can be viewed as the main factor contributing to rock uplift, their present-day topography being the result of the competition between tectonic and erosional processes (e.g., England and Molnar, 1990; Bishop, 2007). In the same way, topography, drainage pattern analysis, and geomorphic features can be used to evaluate recent and present-day tectonic activity (e.g., Keller et al., 2000; Azor et al., 2002; Molin et al., 2004; Bull, 2007; Pérez-Peña et al., 2009a).

The drainage pattern in tectonically active regions is very sensitive to active processes such as folding and faulting. These processes can be responsible for accelerated river incision, asymmetries of the catchments, and river diversions, among other effects (e.g., Cox, 1994; Jackson et al., 1998; Clark et al., 2004; Salvany, 2004; Schoenbohm et al., 2004). River incision in such regions is related to tectonic uplift, although other processes such as stream piracy, base-level lowering, and climatic episodes are also responsible for differential and accelerated river incision (e.g., Hancock and Anderson, 2002; Starkel, 2003; Azañón et al., 2005). Numerical dating of geomorphic surfaces and/or recent deposits is always necessary in order to obtain rates for the tectonic (folding, faulting, etc.) and geomorphic (river incision,

* Corresponding author.
E-mail address: vperez@ugr.es (J.V. Pérez-Peña).

0169-555X/$ – see front matter © 2010 Elsevier B.V. All rights reserved.
doi:10.1016/j.geomorph.2010.02.020

etc.) processes (e.g., Hetzel et al., 2002; Watchman and Twidale, 2002; Pérez-Peña et al., 2009b).

This paper aims to evaluate the Quaternary tectonic activity in the Sierra Nevada mountain range (SE Spain) by drawing on geomorphic indexes and drainage pattern analysis. The area of study is located in the central part of the Betic Cordillera which represents, together with the Rif in Northern Morocco, the westernmost fragment of the Alpine circum–Mediterranean orogenic belt. The geomorphic data obtained suggest that tectonic activity in this mountain range is concentrated along the western mountain front where normal fault scarps are well developed, although transverse active folding is also deduced and compatible with some of the tectonic models proposed recently (Martínez-Martínez et al., 2002, 2006).

2. Geologic and tectonic setting

The Betic–Rif arc-shaped mountain belt (Fig. 1) constitutes the western termination of the peri-Mediterranean Alpine orogen, being related on a broad scale to the collision between Africa and Iberia (de Mets et al., 1994; Morales et al., 1999; Galindo-Zaldívar et al., 1999, 2003). Despite the general N–S compressional setting, the kinematic picture of this orogenic belt is rather complicated because of the presence of a micro-plate (Alborán Domain) which seems to have displaced westward, colliding in Early Miocene times with the margins of southern Iberia and northern Africa (Balanyá and García-Dueñas, 1988). Thus, the Betic–Rif cordillera is made up of two external zones (the South Iberian margin in Spain and the Maghrebian margin in northern Morocco) with one internal zone in-between (the Alborán domain). The early compressional tectono-metamorphic evolution of the Alborán Domain is obscured by pervasive extensional tectonics which occurred since Early–Middle Miocene times (e.g. Galindo-Zaldívar et al., 1989; Platt and Vissers, 1989; García-Dueñas et al., 1992; Lonergan and Platt, 1995; Martínez-Martínez et al., 1997; Orozco et al., 2004). This extensional tectonics is responsible for ductile shear zones and low- and high-angle normal faults, as well as for the initial development of Neogene–Quaternary sedimentary basins. The largest of these sedimentary basins is the Alborán Sea (Watts et al., 1993; Comas et al., 1999) which was formed over the metamorphic rocks of the internal zone, separating the Rif in Northern Morocco from the Betics in Southern Spain (Fig. 1). The extensional tectonics seem to have occurred coevally with N–S oriented compressional structures also active since the Late Miocene and responsible for large-scale E–W oriented folds (Martínez-Martínez et al., 2002). These folds are responsible for the most outstanding topographic features in the internal zone of the Betic Cordillera: the antiforms coincide with the main ranges, which, thus, can be said to be antiformal ridges, and the synforms coincide with Neogene–Quaternary sedimentary basins (Fig. 1).

The Sierra Nevada mountain range (Fig. 2) has been considered as an orogenic dome or core-complex structure (Davis, 1980; Davis et al., 2004), having been exhumed since the Late Miocene in an extensional tectonic regime involving, in a first stage, both low-angle normal faulting and vertical ductile thinning (Galindo-Zaldívar et al., 1989; Martínez-Martínez et al., 2004). The Pliocene–Quaternary tectonic evolution is responsible for the formation of a large-scale open antiformal ridge coincident with the whole extent of the Sierra Nevada and coeval normal faulting (Fig. 2). Galindo-Zaldívar et al. (2003) considered the antiformal ridge related to a blind-thrust buried under the northern E–W oriented mountain front of the Sierra Nevada, while the normal faults would be coeval and related to extension sub-perpendicular to the NNW–SSE axis of maximum shortening (Africa–Iberia present-day vector of convergence). Martínez-Martínez et al. (2004) proposed that the present-day topography of the Sierra Nevada is due to the interference of two orthogonal sets of Miocene–Pliocene, large-scale open folds trending roughly E–W and NNE–SSW. They suggested that the NNE–SSW folds were

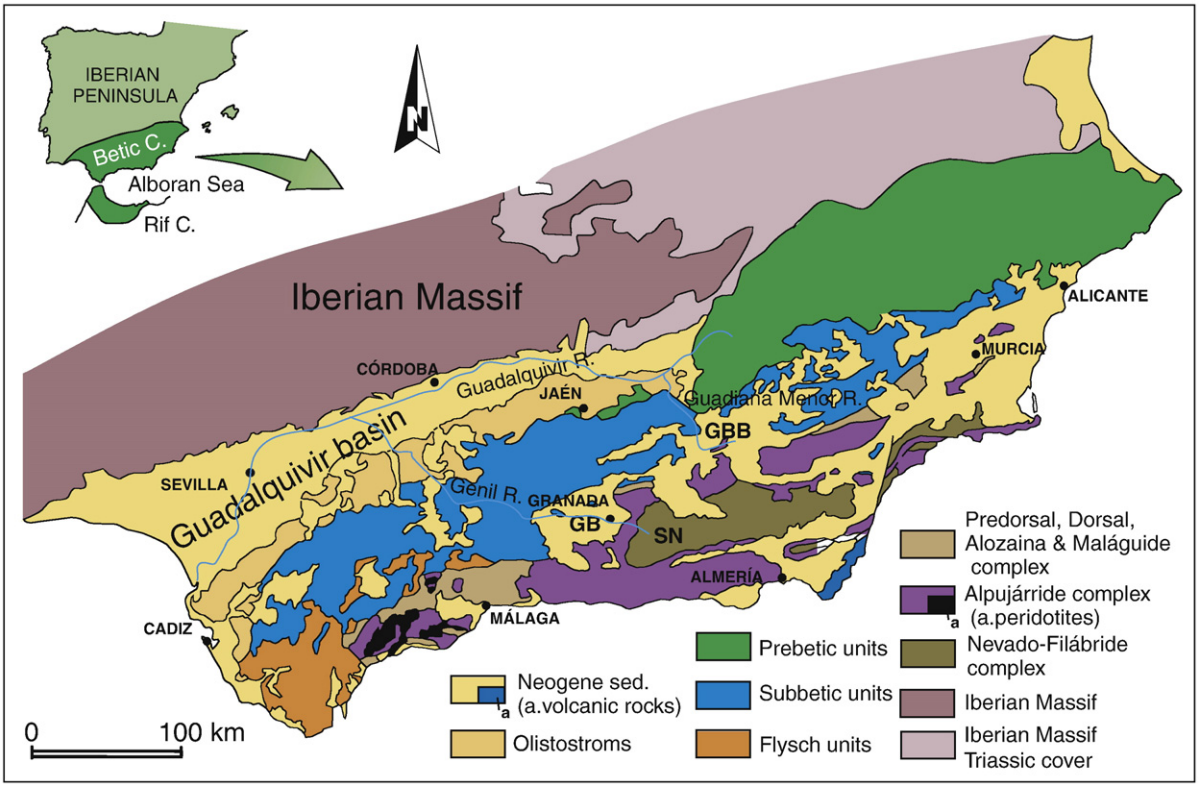

Fig. 1. Geological sketch of the Betic Cordillera (modified from Ruano, 2003). GB — Granada basin; GBB — Guadix–Baza basin; SN — Sierra Nevada. The inset shows the Betic–Rif Cordillera and the Alborán Sea.

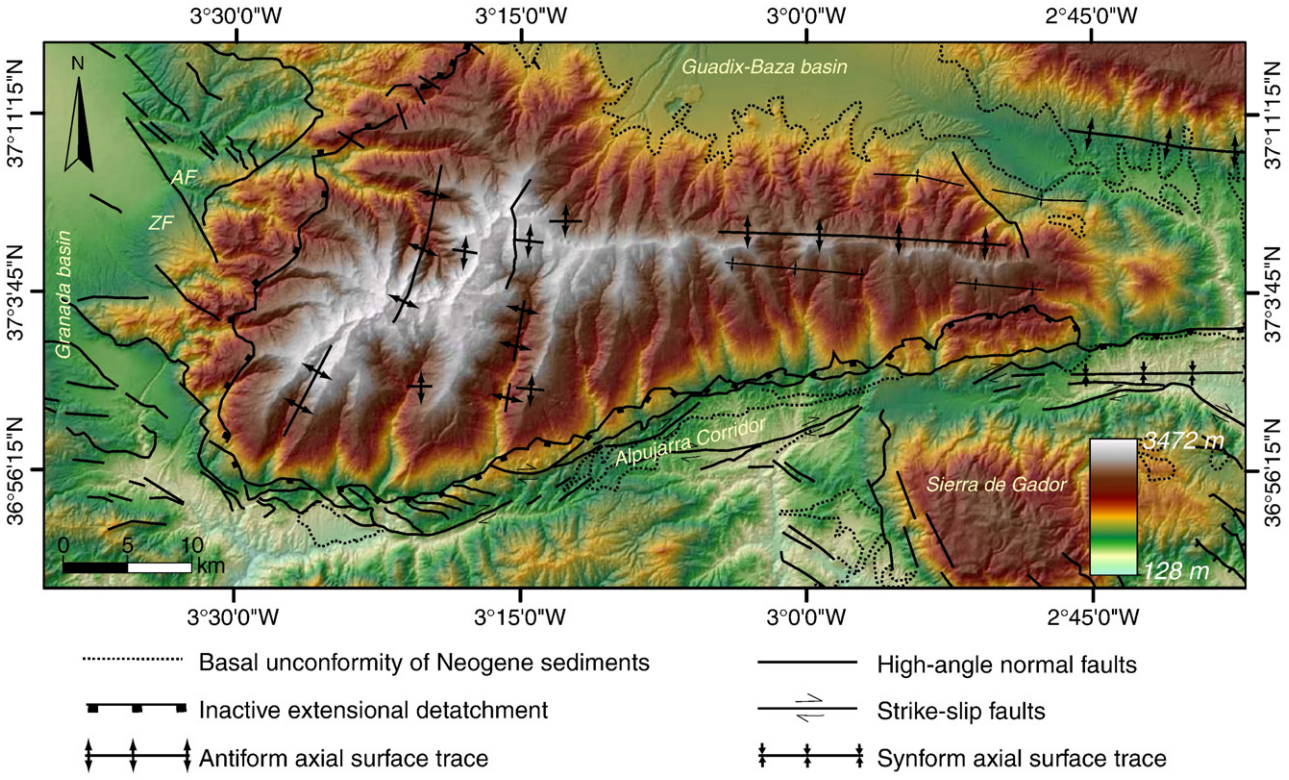

Fig. 2. Digital elevation model (DEM) with the Sierra Nevada and the main tectonic structures. Slightly modified from Martínez-Martínez et al. (2006). AF — Alhambra Formation, ZF — Zubia Formation (see text for further explanation).

generated by a rolling-hinge mechanism, while the E–W folds were formed by shortening perpendicular to the direction of extension.

The western border of the Sierra Nevada is bounded by NW–SE striking normal faults (Fig. 2) which limit the sediments of the Neogene–Quaternary Granada sedimentary basin. These faults clearly indicate an activity in the Quaternary including the Holocene, as can be deduced from seismicity and deformed Holocene alluvial fans (Calvache et al., 1997; Alfaro et al., 2001; Viseras et al., 2003). Some authors have proposed slip rates of 0.6–0.8 mm yr^{-1} for these faults in the Quaternary (Sanz de Galdeano, 1996; Keller et al., 1996). El Hamdouni et al. (2008) studied some geomorphic indexes in this part of the Sierra Nevada, proposing a moderate-high tectonic activity for these faults in the Quaternary. Reinhardt et al. (2007) studied the response to a rapid base-level fall in the Torrente River (basin number 31, Fig. 3), which is limited in its mouth by these faults. These authors dated Quaternary sediments using radiometric methods and proposed that 50 m of base-level fall must have occurred in the last 21 ka.

The northern and southern borders of the Sierra Nevada present very different characteristics. The southern border is bounded by a WSW–ENE sub-vertical dextral strike-slip fault zone which has been active since the Miocene (Sanz de Galdeano, 1985; Martínez-Martínez et al., 2006). On the contrary, the northern border of the Sierra Nevada corresponds with the northern limb of an E–W fold, with the Neogene–Quaternary sediments of the Guadix–Baza basin unconformably overlaying the metamorphic rocks of the Sierra Nevada (Fig. 2).

The aforementioned Granada and Guadix–Baza basins are two of the largest Neogene–Quaternary basins in the central part of the Betic Cordillera. These two basins have quite similar sedimentary records, with marine Tortonian sediments unconformably overlaid by continental Pliocene–Quaternary sediments (Soria et al., 1998). During the Quaternary, these two basins changed from an internal drainage, attested to by the lacustrine sediments that constitute the uppermost part of the sedimentary sequence, to an external drainage to the Atlantic Ocean via the Guadalquivir River (the biggest river in south Spain, Fig. 1). Despite these similarities, the Quaternary geomorphic evolution and the present-day topography of the Guadix–Baza and Granada basins are quite different, probably being linked to the recent tectonics of the Sierra Nevada.

The Guadix–Baza basin's present-day topography consists of a high plateau with a mean altitude of 1000 m, intensively dissected by the river network (Pérez-Peña et al., 2009b). Its Late Quaternary evolution is mostly dominated by erosional processes following its capture by the Guadalquivir River (Azañón et al., 2005). In contrast, the Late Quaternary evolution of the Granada basin is dominated by active normal faulting along its northeastern border, where the maximum relief is concentrated. The remainder of the basin has a mean altitude of ~700 m, being scarcely incised by the fluvial network (Pérez-Peña et al., 2009c).

The present-day seismicity in the Sierra Nevada and surrounding areas fits well with the tectonic structures. Earthquake epicentres are concentrated along the western and southern borders, the core of the range being aseismic (Martínez-Martínez et al., 2006). The Granada basin, located to the west of the Sierra Nevada (Figs. 1 and 2), presents the highest seismic activity in all of the Iberian Peninsula, with a great number of earthquakes of low to moderate magnitude ($M_b \leq 5.5$; de Miguel et al., 1989). Focal mechanisms indicate a present-day stress-state dominated by radial extension or by an NE–SW oriented extensional axis (Galindo-Zaldívar et al., 1999; Muñoz et al., 2002).

3. Drainage pattern analysis

Uplift of the Sierra Nevada started in Early Tortonian times (Johnson, 1997; Braga et al., 2003), but its present-day drainage pattern started to develop in the Pleistocene, i.e., streams draining the Sierra Nevada incised into Pleistocene deposits of the Neogene basins surrounding the range. Nevertheless, some palaeorivers

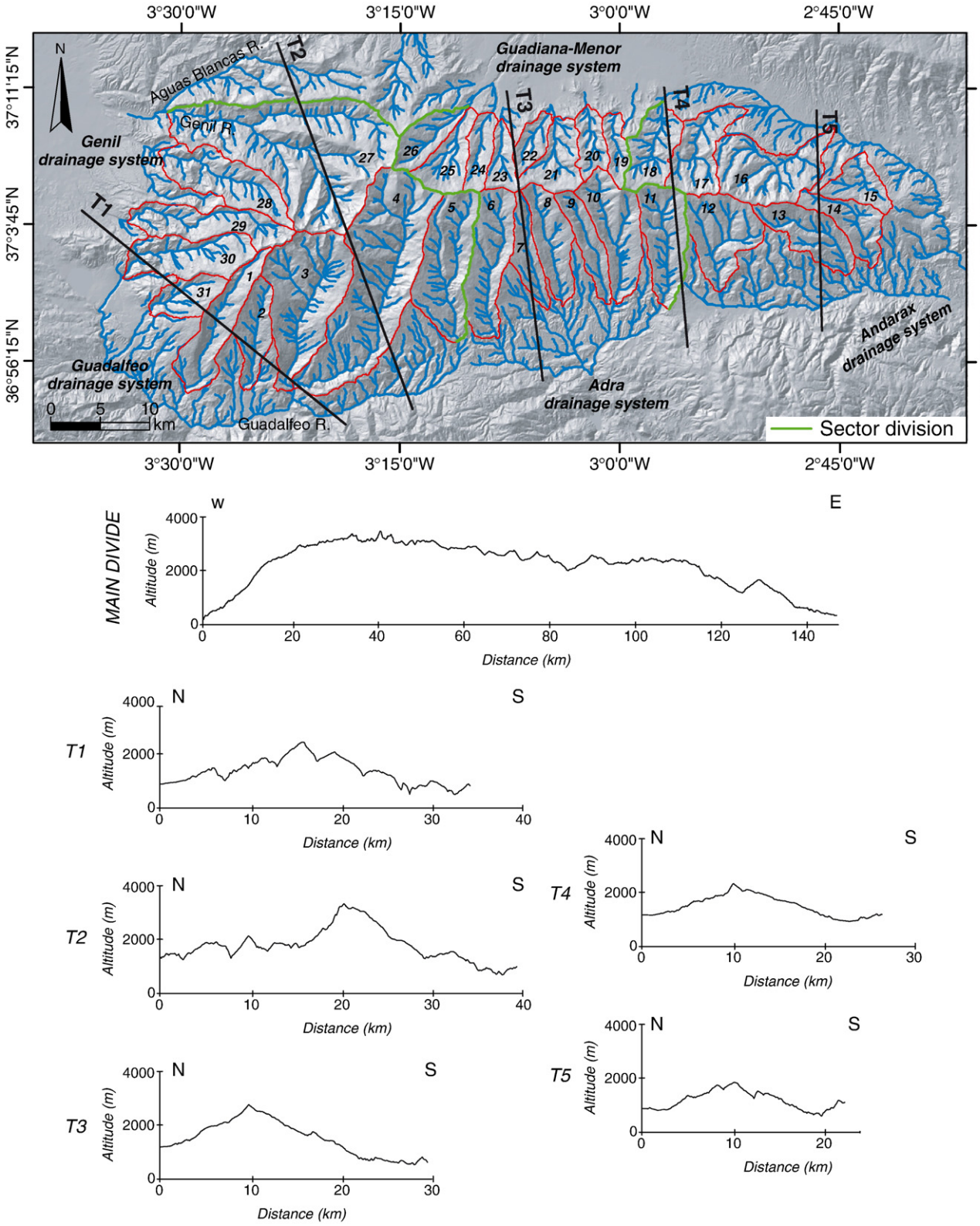

Fig. 3. Shaded relief map with the drainage network extracted for the Sierra Nevada. Numbers indicate the selected basins (see Table 2 for river names). Five main drainage systems are indicated: Genil (basins 27, 28, and 29), Guadalfeo (basins 1, 2, 3, 4, 5, 30, and 31), Adra (basins 6, 7, 8, 9, 10, and 11), Andarax (basins 12, 13, 14, 15, 16, 17, and 18), and Guadiana Menor (basins 19, 20, 21, 22, 23, 24, 25, and 26). Five transversal profiles and one longitudinal profile (following the main divide between the northern and southern slopes) are presented. The profiles were made using a 10-m DEM (vertical exaggeration × 6.5 for the longitudinal profile and × 3.3 for the transversal profiles).

coincide with modern rivers, as deduced from the distribution of Pliocene to lower Pleistocene fan deposits in the Granada basin (Alhambra Formation and Zubia Formation, Fig. 2) and the Alpujarra Corridor (Fig. 2).

The drainage network has been extracted from a Digital Elevation Model (DEM) with a 10-m resolution following the methodology described by Tarboton (1997). This methodology takes into account the accumulation of upwards curved grid cells (Peuker and Douglas,

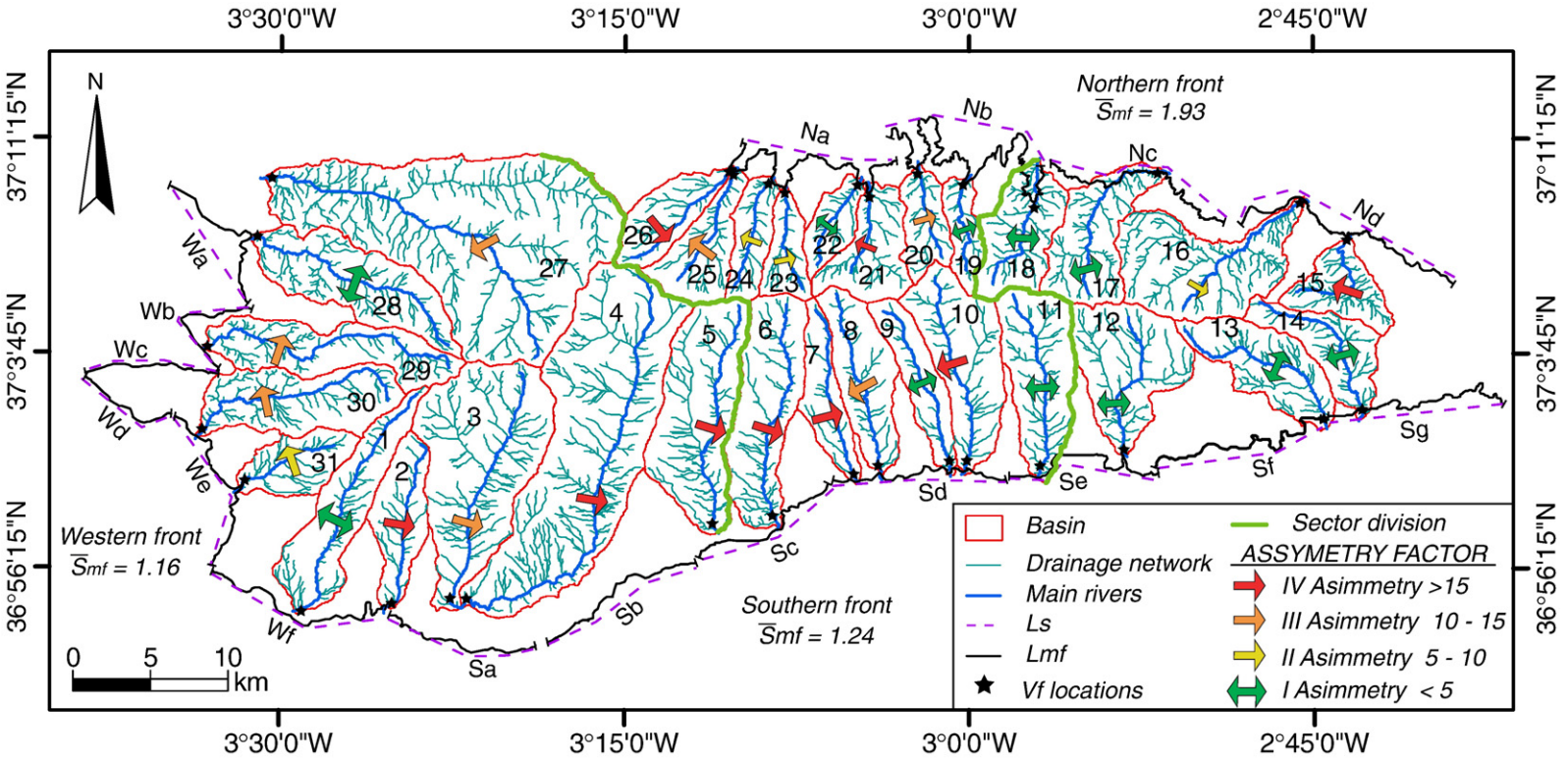

Fig. 4. Schematic map showing the main geomorphic indexes calculated in this work. *AF* values are represented with an arrow indicating the asymmetry sense and colour indicating the class (see text for further explanation). Black stars show the locations of the V_f measurements (300 m upstream from the mountain front). Bold green lines mark the eastern, central, and western Sierra Nevada sectors differentiated for the hypsometric curve study. Segments for S_{mf} calculation are indicated (W — western front segments, S — southern front segments, N — northern front segments), and the values are shown in Table 1. Basins have been labeled with a number (see Table 1 for river names).

Table 1
S_{mf} values for the different mountain front segments (see location in Fig. 4). Mean values for each main front are also indicated.

Front	Segment	S_{mf}	Mean S_{mf}
West	Wa	1.39	1.16
	Wb	1.01	
	Wc	1.01	
	Wd	1.03	
	We	1.28	
	Wf	1.29	
South	Sa	1.09	1.24
	Sb	1.12	
	Sc	1.15	
	Sd	1.21	
	Se	1.35	
	Sf	1.43	
	Sg	1.34	
North	Na	2.46	1.93
	Nb	3.49	
	Nc	1.31	
	Nd	1.23	

Table 2
Values of V_f (valley floor width-to-height ratio) and *AF* (asymmetry factor) for the main rivers of the Sierra Nevada.

Basin	River name	V_{fw}	E_{ld}	E_{rd}	E_{sc}	V_f	*AF*
1	Lanjarón R.	44	1157	710	539	0.112	3.872
2	Chico R. (W)	71	800	653	553	0.409	16.665
3	Poqueira R.	19	937	864	604	0.064	13.701
4	Trevelez R.	15	1195	807	633	0.041	22.110
5	Cadiar R.	78	1284	1261	1012	0.299	23.851
6	Mecina R.	18	1271	1053	862	0.060	20.716
7	Valor R.	55	877	865	780	0.604	21.697
8	Nechite R.	40	1028	980	803	0.199	11.566
9	Laroles R.	74	1006	828	731	0.398	2.850
10	Picena R.	66	884	935	706	0.324	15.189
11	Alcolea R.	98	1114	1052	797	0.343	3.350
12	Andarax R.	54	1316	1333	959	0.148	3.777
13	Chico R. (E)	30	894	945	660	0.116	4.927
14	Rmb. de Tices	73	834	822	635	0.378	2.083
15	Rmb. de Santillana	78	948	996	778	0.402	18.100
16	Abrucena R.	175	919	1054	834	1.148	8.854
17	Nacimiento R.	92	1101	1217	1008	0.609	0.408
18	Hueneja R.	144	1366	1405	1194	0.752	2.982
19	Rmb. De los Castaños	61	1540	1486	1313	0.305	1.140
20	Chico creek	108	1392	1360	1273	1.049	14.399
21	Rmb. de Benejar	45	1464	1364	1279	0.333	21.957
22	Bco. del Gallego	91	1378	1395	1272	0.795	0.847
23	Bco. del Barrio	52	1447	1485	1373	0.559	9.828
24	Bco. del Pueblo	37	1522	1500	1344	0.222	6.449
25	Bco. de Alcazar	33	1546	1381	1294	0.195	10.975
26	Bco. de Alhorí	20	1395	1417	1330	0.263	24.541
27	Genil R.	185	970	933	766	0.997	10.040
28	Monachil R.	23	1098	1206	948	0.113	3.599
29	Dilar R.	26	1223	1237	957	0.095	11.816
30	Durcal R.	28	1132	1103	809	0.091	11.049
31	Torrente R.	19	1373	1277	974	0.054	8.327

1975; Band, 1986), being adaptive to spatial variability in drainage density. This drainage network was cleaned and validated in order to avoid DEM-associated errors, and channels were ordered following Strahler (1952).

We have divided the Sierra Nevada in three sectors (west, middle, and east), according to the main drainage systems. The western sector comprises the Genil and Guadalfeo drainage systems with their corresponding tributaries (Fig. 3). The Guadalfeo drains to the Mediterranean Sea, while the Genil River (Fig. 1) is the main tributary of the Guadalquivir River, which, in turn, drains to the Atlantic Ocean. The middle sector contains the Adra drainage system on the southern slope of the Sierra Nevada, which drains towards the Mediterranean Sea and some tributaries of the Guadiana–Menor River (tributary of Guadalquivir River, Fig. 1) in the northern slope, which drains to the Atlantic Ocean (Fig. 3). The eastern sector includes the Andarax drainage system which drains towards the Mediterranean Sea (Fig. 3).

The main divide in the Sierra Nevada is mostly straight or gently curved, with the highest elevations located in its western part (Fig. 3). Some bends of the crest-line are clearly related to headward erosion of streams draining the southern limb of the Sierra Nevada which may capture the highest sectors of the catchments draining the northern limb (Fig. 3). The streams draining the northern limb are generally shorter than those draining the southern limb, due to the higher local base-level. The orientations of the main streams are generally perpendicular to the crest-line in the middle sector of the range and present a radial pattern in the western termination. The drainage pattern in the easternmost sector of the Sierra Nevada presents some peculiar anomalies. There are some channels that flow almost parallel to the divide, coinciding with the traces of minor E–W oriented folds.

4. Geomorphic indexes

We have analyzed three geomorphic indexes: mountain front sinuosity (S_{mf}), valley floor width-to-height ratio (V_f), and asymmetry factor (*AF*), together with topographic river profiles and hypsometric curves for the main catchments of the Sierra Nevada.

4.1. Mountain front sinuosity (S_{mf})

Mountain front sinuosity (S_{mf}) was defined by Bull (1977) as:

$$S_{mf} = \frac{L_{mf}}{L_s} \quad (1)$$

where L_{mf} is the length of the mountain front along the foot of the mountain, i.e., the topographic break in the slope, and L_s is the length of the mountain front measured along a straight line. This index has been used to evaluate the relative tectonic activity along mountain fronts (Bull and McFadden, 1977; Keller and Pinter, 2002; Silva et al., 2003; Bull, 2007). In active mountain fronts, uplift will prevail over erosional processes, yielding straight fronts with low values of S_{mf}. Along less active fronts, erosional processes will generate irregular or sinuous fronts with high values of S_{mf}. Some studies have proposed that the values of the S_{mf} index lower than 1.4 are indicative of tectonically active fronts (Keller, 1986; Silva et al., 2003).

This index has been previously applied to some of the fault-bounded mountain fronts of the western Sierra Nevada, yielding low values (Martín-Rojas et al., 2001; El Hamdouni et al., 2008). In this work, we have calculated the S_{mf} index for the western, northern, and

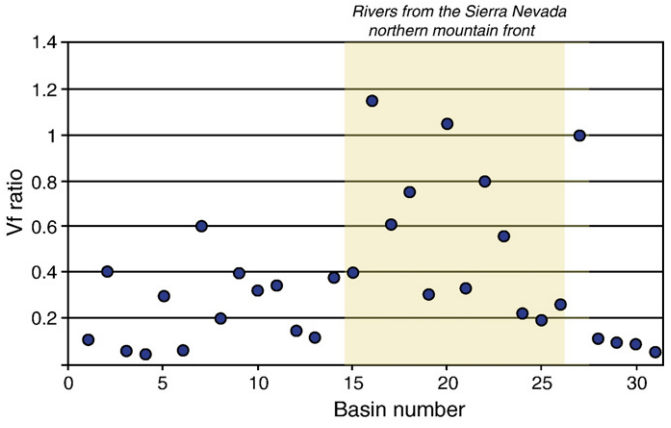

Fig. 5. Plot of V_f values for the main rivers of the Sierra Nevada. River names and locations are shown in Fig. 4 and Table 2.

southern mountain fronts of the Sierra Nevada (Fig. 4, Table 1) which corresponds to different tectonic environments. Lateral variations in the S_{mf} values occur because the selected mountain fronts are quite long (40–80 km). To detect such possible lateral variations, we have calculated the S_{mf} index for mountain front segments of about 10 km.

The mean values of the S_{mf} index are low in the western (1.16) and southern (1.24) mountain fronts (Fig. 4, Table 1), suggesting that they are tectonically active. On the contrary, the mean S_{mf} value obtained for the northern mountain front is relatively high (1.93), thus confirming a relatively low tectonic activity, consistent with other geomorphic and tectonic features. With respect to lateral variations of S_{mf}, only the southern mountain front shows slight systematic variations. Individual values of S_{mf} for 10 km-long segments along this mountain front decrease slightly westward (Table 1). This is consistent with a higher level of tectonic activity of the southern mountain front westward, as suggested by some authors (e.g., Martínez-Martínez et al., 2006).

4.2. Valley floor width-to-height ratio (V_f)

Valley floor width-to-height ratio (V_f) (Bull and McFadden, 1977) is a geomorphic index conceived to discriminate between V-shaped and U-shaped flat-floored valleys. This index is defined as:

$$V_f = \frac{2V_{fw}}{E_{ld} + E_{rd} - 2E_{sc}} \quad (2)$$

where V_{fw} is the width of the valley floor, E_{ld} and E_{rd} are elevations of the left and right valley divides, respectively, and E_{sc} is the elevation of the valley floor.

Deep V-shaped valleys ($V_f<1$) are associated with linear, active downcutting streams characteristic of areas subjected to active uplift, while flat-floored valleys ($V_f>1$) indicate an attainment of the base-level of erosion mainly in response to relative tectonic quiescence (e.g. Keller and Pinter, 2002, Bull, 2007, 2009a,b). This index has been applied to several mountain fronts located in the eastern and central Betic Cordillera (Silva et al., 2003; Pedrera et al., 2009).

The V_f index was calculated for all the main channels, 300 m upstream from the mountain front (Fig. 4). For narrow river-valleys (valley-width<50 m), the DEM is insufficient to accurately measure valley widths. Therefore, V_f was determined by measuring widths directly from aerial photographs. V_f values are higher in the northern mountain front (Table 2), with the lower values concentrated along the western mountain front (Fig. 5). A special case in the western front is the Genil River (basin number 27). The catchment for this river was drawn only until the confluence with Aguas Blancas River (that does not drain the Sierra Nevada range; Fig. 3). For this reason the values of V_f are not calculated in a mountain front, but in this river confluence. This fact can explain that this river presents the highest V_f value of the eastern front, where low values are concentrated.

4.3. Asymmetry factor (AF)

The asymmetry factor (*AF*) of catchments was used to detect possible tectonic tilting at the scale of the whole range. The *AF* is defined as (Hare and Gardner, 1985; Keller and Pinter, 2002):

$$AF = \frac{A_R}{A_T} \times 100 \quad (3)$$

where A_R is the area of the basin to the right (facing downstream) of the trunk stream, and A_T is the total area of the drainage basin. Values of *AF* above or below 50 indicate that the basin is asymmetric.

In order to avoid possible confusions between the catchments located in the northern and southern slopes of the Sierra Nevada, we expressed *AF* as the absolute value minus 50, with an arrow indicating the asymmetry direction in Fig. 4.

$$AF = \left| 50 - \frac{A_R \times 100}{A_T} \right|. \quad (4)$$

We have divided *AF* absolute values in four classes: $AF<5$ (symmetric basins), $AF=5$–10 (gently asymmetric basins), $AF=10$–15 (moderately asymmetric basins), and $AF>15$ (strongly asymmetric basins). *AF* values in the western part of the Sierra Nevada present a pattern with contrary asymmetries at both sides of the Lanjarón River (1), thus coinciding with the fold hinge of one of the NNE–SSW oriented antiforms (Table 1, Fig. 4). In the eastern part of the Sierra Nevada, there is no defined pattern in *AF* values, with the majority of the basins being symmetric ($AF<5$).

4.4. Hypsometric curves

The hypsometric curve of a catchment represents the distribution of area and altitude within it (Strahler, 1952). In this study, the curves have been depicted by plotting the relative area (0–1) above each relative height (0–1). A useful attribute of these curves is that drainage basins of different sizes can be compared, since area and elevation are plotted as functions of total area and total elevation (Keller and Pinter, 2002; Walcott and Summerfield, 2008; Pérez-Peña et al., 2009c). The shape of this curve is related to the degree of dissection of the basin, i.e., its erosional stage. Convex hypsometric curves characterize relatively "young" weakly eroded regions, S-shaped curves characterize moderately eroded regions, and concave curves characterize relatively "old" highly eroded regions. The area below the hypsometric curve is known as the hypsometric integral (*HI*), varying from 0 to 1, with values close to 0 in highly eroded regions and values close to 1 in weakly eroded regions. The shape of the hypsometric curves (and the *HI* values) also provides valuable information about the tectonic, climatic, and lithological factors controlling catchment landscape (e.g., Moglen and Bras, 1995; Willgoose and Hancock, 1998; Huang and Niemann, 2006).

We calculated hypsometric curves for all of the basins draining the Sierra Nevada with the aid of an ArcGIS extension (Pérez-Peña et al., 2009d). The hypsometric curves show differences between the curves of the northern and southern slopes of the Sierra Nevada. The curves from the northern slope (northwards to the Lanjarón River (1)) present more concave shapes than the ones from the southern slope (Fig. 6). There is not a clear variation in the shape of the curves from east to west in either the northern or southern slopes of the Sierra Nevada.

4.5. Longitudinal river profiles

Longitudinal river profiles can be interpreted as resulting from the balance between rates of erosion and uplift (Schumm et al., 2000; Hovius, 2000; Keller and Pinter, 2002; Menéndez et al., 2008; Bull 2009b). Hovius (2000) defined three types of profile morphologies according to uplift rates and monthly rainfall (as a proxy of denudation rate). Concave profiles represent long-term equilibrium between uplift and erosion rates. Concave–convex profiles with erosion steps in the middle reaches indicate long-term predominance of erosional processes. Convex profiles are characteristic of areas where uplift (active tectonics) is dominant.

Valuable information can also be obtained from "ridge-line profiles" (Menéndez et al., 2008). These profiles are drawn by projecting rivers onto a theoretical pre-incision surface that is obtained by interpolating the altitudes from present-day lateral divides of the basins (Menéndez et al., 2008; Fig. 7). One advantage of ridge-line profiles is that they have lengths equivalent to the river longitudinal profile. However, the estimated pre-incision surface cannot be considered to be the precise pre-incision surface

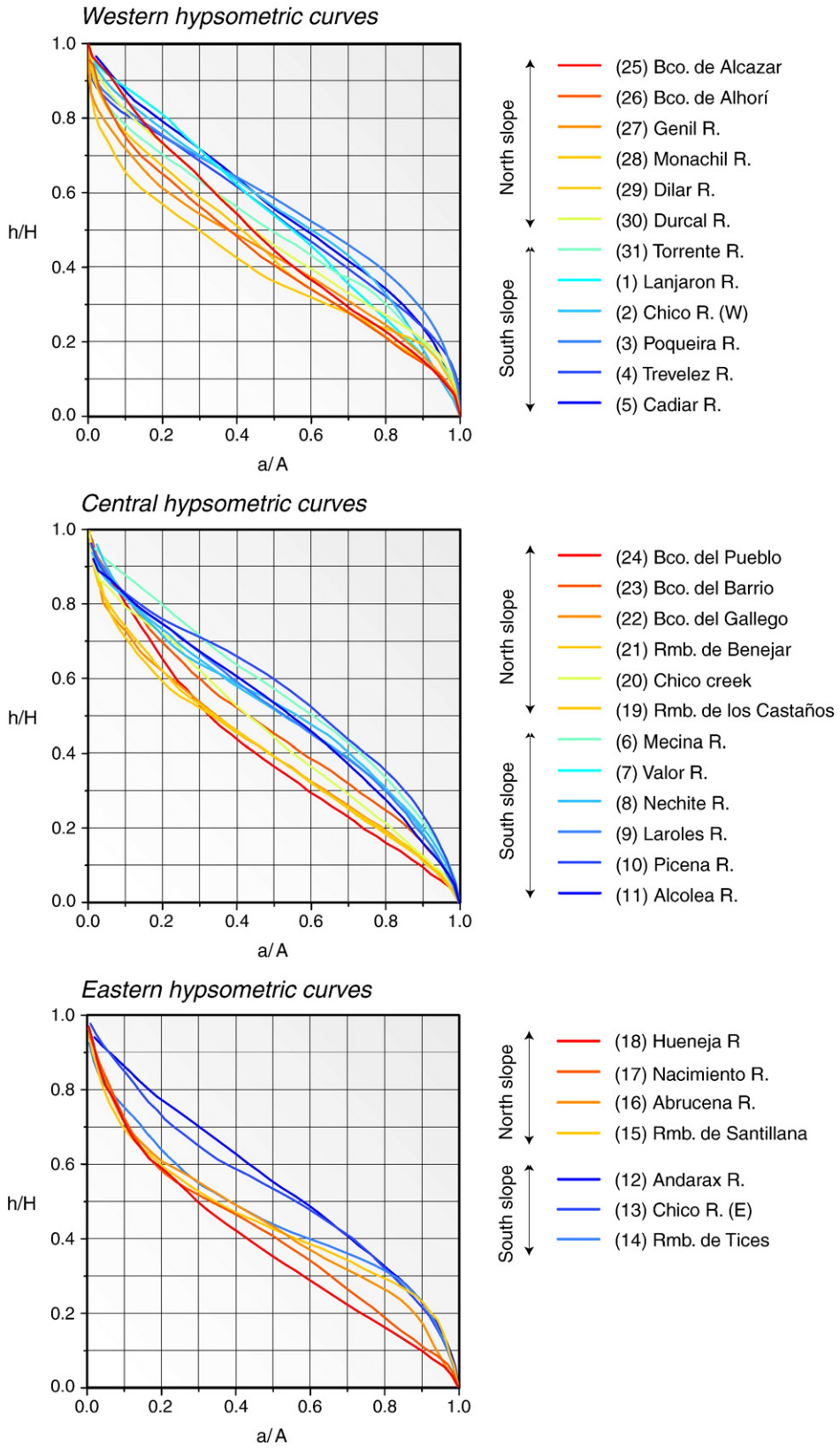

Fig. 6. Hypsometric curves for the eastern, central, and western sectors of the Sierra Nevada. Curves have been calculated using a 10-m DEM and CalHypso ArcGIS module (Pérez-Peña et al., 2009d). Curves from the northern slope of the Sierra Nevada are in blue, while curves from the southern slope are in red.

(Brocklehurst and Whipple, 2002). Nevertheless, these profiles can generate a view of the structure of the relief for each basin, allowing relative comparisons of bulk erosion between the different basins.

Longitudinal and ridge-line river profiles have been extracted for the main rivers draining the Sierra Nevada (Fig. 8). The rivers of the northern slope of the Sierra present mainly concave profiles, while the

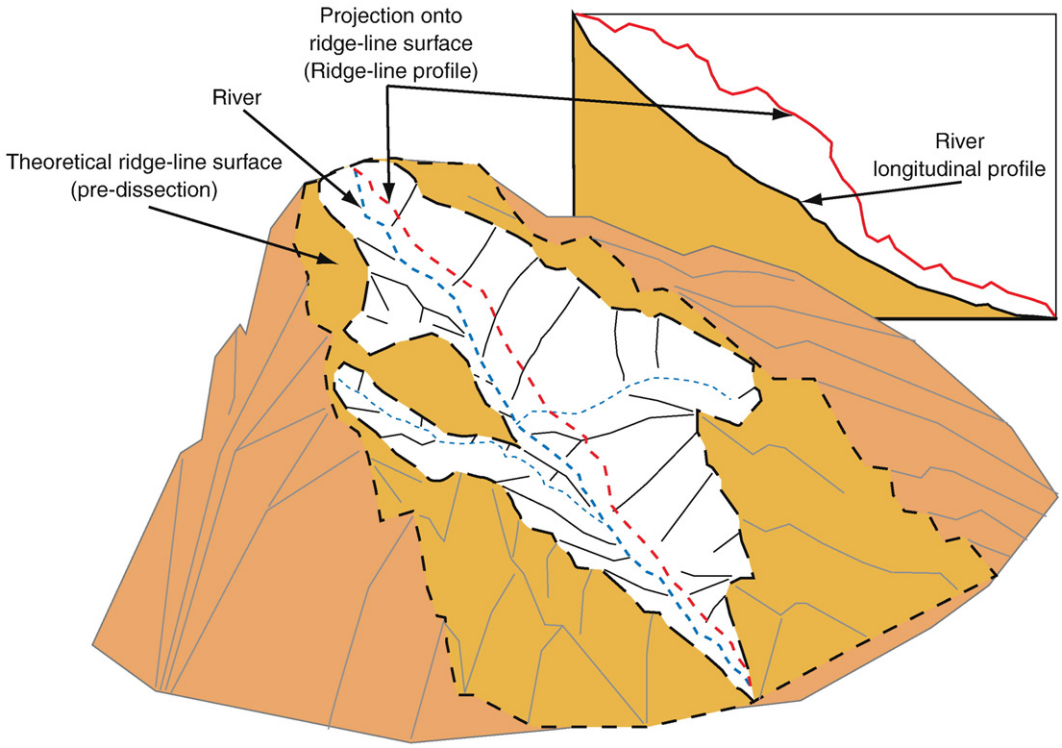

Fig. 7. Schematic illustration showing the methodology used to obtain the projected ridge-line profiles. Slightly modified from Menéndez et al. (2008). The ridge-line surface is obtained by interpolating the altitudes from the two lateral divides of the basin.

rivers of the southern slope have linear and convex profiles (Fig. 8). In the western sector, some river profiles show erosion steps [the Poqueira (3), Trevélez (4), and Cádiar (5) rivers], while others present clearly convex profiles [the Lanjarón River (1)] or slightly concave profiles [the Dúrcal (30), Monachil (28), and Dílar (29) rivers] (Fig. 8). Ridge-line profiles show the greatest height differences in the western sector of the Sierra Nevada (Fig. 8). On the contrary, the smallest height differences are found in rivers on the northern slope (Fig. 8).

5. Discussion

The geomorphic indexes calculated in this work suggest that the Sierra Nevada is tectonically active, with the more recent uplift concentrated along its western mountain front, where S_{mf} and V_f present the lowest values (Figs. 4 and 5). This is corroborated by surface geology, since the western mountain front coincides with prominent normal fault scarps and has associated Late Pleistocene–Holocene alluvial fans (Calvache et al., 1997). Furthermore, these alluvial fans show tectonic controls on their sedimentary patterns and geometries, having width-length ratios >1 and absence of incised channels (Calvache et al., 1997; Viseras et al., 2003). These normal faults present high Quaternary slip rates (Sanz de Galdeano 1976, 1996; Keller et al., 1996). The distribution of present-day seismicity also points to active faulting along the western mountain front of the Sierra Nevada (Morales et al., 1997; Muñoz et al., 2002; Martínez-Martínez et al., 2006).

The southern mountain front of the Sierra Nevada is characterized by low values of S_{mf} and V_f (Figs. 4 and 5), with S_{mf} values increasing eastward. Despite the lack of Quaternary absolute ages, the landscape of this mountain front seems to be older than the one of the western mountain front. In this regard, the absence of Quaternary alluvial fans along this southern mountain front must be stressed, with the present-day drainage network well hierarchized and entrenched into the Neogene sediments of the Alpujarran Corridor (Fig. 3). This fact could be indicative of a gradual response to late Neogene–Quaternary uplift of this sector as a whole. Furthermore, the southern mountain front runs parallel to one of the main drainage systems in the region, namely the Guadalfeo River, whose Quaternary incision and mountain front retreat might be responsible, at least partially, for the low values of S_{mf} and V_f. Moreover, fault scarps are not as prominent as in the western mountain front. However, the presence of sub-vertical strike-slip faults along some segments of this mountain front (Sanz de Galdeano and Rodríguez-Fernández, 1985) is indicative of a recent tectonic activity. In this respect, Martínez-Martínez et al. (2006) proposed that the southern Sierra Nevada border is an active transfer fault composed of strike-slip fault segments, which join two normal fault-bounded mountain fronts: western Sierra de Gádor and western Sierra Nevada. Interestingly, the eastern higher S_{mf} values might be related to this tectonic scenario, representing the inactive part of this southern mountain front eastward of the Sierra de Gádor active mountain front. Nevertheless, the differences in the S_{mf} values could be not big enough to completely support this idea.

The northern mountain front corresponds to the northern limb of the E–W antiformal ridge of the Sierra Nevada, with the Neogene–Quaternary sedimentary infill of the Guadix–Baza basin lying unconformably over the metamorphic rocks of the Sierra Nevada This front has the highest S_{mf} and V_f values, suggesting low rates of tectonic activity, and thus pointing to an inactive fold limb during the Quaternary. Furthermore, no appreciable present-day seismicity is observed along this mountain front, which suggests tectonic inactivity. Nevertheless, the high topography of the Guadix–Baza basin suggests a substantial uplift in recent times (Pérez-Peña et al., 2009b). One possible scenario for this northern mountain front is one with the Guadix–Baza basin and the Sierra Nevada range being uplifted together as a single block in Quaternary times (see below).

Geomorphic indicators indicative of active tectonics, including hypsometric curves, longitudinal river/ridge-line profiles, and drainage patterns, have subtle E–W and N–S variations. N–S variations are mainly due to the fact that the local base-level is ≈1100 m in the northern mountain front of the Sierra Nevada and ~600 m in the

southern front, i.e., southern slope streams have more erosional power than northern ones. Therefore, southern slope streams are longer and more entrenched than northern ones (Figs. 3 and 4). These differences in base-level altitudes could be the response to a differential tectonic uplift of the northern mountain front with respect to the southern one. No systematic E–W variation in the hypsometric curves is found in the Sierra Nevada (Fig. 6). On the contrary, river entrenchment as deduced from the comparison of longitudinal and ridge-line river profiles increases westward (Fig. 8). This fact might result from recent uplift of the western Sierra Nevada.

The main rivers of the western and central sectors of the Sierra Nevada have a radial pattern around the highest peaks (Figs. 3 and 4). This simple pattern changes in the easternmost sector where some streams are not perpendicular to the main E–W divide, but, rather, are oblique or even parallel to it (Rivers 13, 14, and 15; Figs. 3 and 4). These streams with "anomalous directions" are probably related to complex piracy processes that occurred during the Pliocene and Quaternary evolution of the Andarax drainage system (Pérez-Peña et al., 2009d). However, E–W oriented active folding might have also contributed to this complicated drainage pattern (Fig. 2).

The asymmetry factor of the main catchments draining the Sierra Nevada has also been calculated in order to detect active, large-scale surface tilting. Most catchments show no asymmetry, except in the southwestern sector of the range where opposite and systematic asymmetries have been found at both sides of the Lanjarón River (1 in Fig. 4). In this sector NNE–SSW-striking faults (parallel to the Lanjarón River) are absent. Therefore, catchment asymmetry in the southwestern sector of the Sierra Nevada is probably due to active folding. From this point of view, an antiform striking parallel to the Lanjarón River (NNE–SSW) accords well with the basin asymmetry data obtained (Fig. 2).

Quaternary uplift rates in the Sierra Nevada are very scarce and do not provide enough data to propose systematic transverse (N–S) and along-strike (E–W) variations. In the eastern sector, García et al. (2003) obtained river incision rates between 0.3 and 0.8 mm yr^{-1} for the last 303–245 ka, which can be reasonably assumed to correspond to tectonic uplift. Actually, these uplift rates (0.3–0.8 mm yr^{-1}) are only slightly higher than long-term uplift rates calculated for the whole period (8–10 Ma) of relief formation in the Sierra Nevada (0.3–0.4 mm yr^{-1}; Sanz de Galdeano and López-Garrido, 1999; Braga et al., 2003; Sanz de Galdeano and Alfaro, 2004). Therefore, the eastern sector of the Sierra Nevada seems to have not undergone accelerated tectonic uplift in the Quaternary. In the western Sierra Nevada, Reinhardt et al. (2007) have reported incision rates of 5 mm yr^{-1}, which they relate to a base-level fall of 50 m in the last 12 ka. The cause of the base-level fall is probably active faulting along the western mountain front of the Sierra Nevada, since sea-level falls did not occur over this period of time. Assuming that these very high erosion rates are due to tectonic uplift in the hanging wall of the normal faults bounding the western Sierra Nevada, the low values of S_{mf} and V_f obtained here are readily explained in terms of the high-rate of recent faulting along this mountain front.

Development of a tectonic model for the Quaternary tectonic evolution of the Sierra Nevada is not an easy task, since extension and compression seem to have acted coevally. Most authors propose a Quaternary stress field characterized by NW–SE compression with a concomitant extension axis oriented NE–SW (de Mets et al., 1994; Galindo-Zaldívar et al. 1999, 2003). Thus, extensional and compressional structures with different orientations would have formed at the same time. In the case of the Sierra Nevada, the E–W oriented, large-scale antiform coincident with the whole range is thought to be a result of the NNW–SSE compression that occurred since the Pliocene, while the NW–SE oriented, normal faults bounding the western mountain front are associated with SW-directed extensional tectonics (e.g., Galindo-Zaldívar et al., 2003). This scenario is roughly consistent with the main conclusions derived from our study, i.e., the highest tectonic activity in the Sierra Nevada is concentrated along its western mountain front and consists in normal faulting with donwthrowing of the SW block (Granada basin) and uplift of the range. Nevertheless, the presence of NNE–SSW oriented active folding in the western termination of the Sierra Nevada, as deduced from the study of catchment asymmetries, and the northern mountain front being inactive introduce some complexity to the tectonic scenario invoked. In this respect, the tectonic model proposed by Galindo-Zaldívar et al. (2003) considered the E–W oriented, large-scale antiformal ridge to be active and related to a blind-thrust buried under the northern mountain front of the Sierra Nevada. Thus, this model envisaged the northern mountain front as tectonically active, which is not the case according to the geomorphic indexes calculated. Our data suggest that this northern limb of the E–W oriented antiformal ridge is inactive and, therefore, the sediments of the Guadix–Baza basin are not separated from the Sierra Nevada metamorphic rocks by any active structure during the Quaternary. Nevertheless, the high average altitude and highly entrenched landscape of this basin indicate that it has been uplifted during the Quaternary (Pérez-Peña et al., 2009b), forming a single block with the Sierra Nevada. Thus, the northern mountain front of the Sierra Nevada seems to be an inherited inactive feature.

At the same time, Galindo-Zaldívar et al. (2003) proposed that SW-directed extension is coeval with the NNW–SSE oriented compression, but their model does not explain the existence of NNE–SSW oriented active folding. These active folds might be completely different in origin from the E–W oriented ones, as proposed by Martínez-Martínez et al. (2006). These authors considered the existence of a generation of NNE–SSW oriented folds with an isostatic origin related to the unroofing produced by the normal faults of the western Sierra Nevada mountain front.

The tectonic model proposed by Martínez-Martínez et al. (2006) explains better the distribution of geomorphic indexes and the topography of the Sierra Nevada and the surrounding Neogene–Quaternary sedimentary basins. The very different topography and landscape of the Granada and Guadix–Baza basins is probably due to the different tectonic locations of the two basins: the Granada basin is located in the hanging wall of the SW-directed extensional system bounding the western the Sierra Nevada and, thus, is subjected to greater Quaternary subsidence. The Guadix–Baza basin, on the other hand, is located in the footwall of the above-mentioned extensional system, being part, together with the whole Sierra Nevada, of a single block suffering tectonic uplift during the Quaternary.

6. Conclusions

The geomorphic indexes calculated in this work indicate that the Sierra Nevada is tectonically active in the Quaternary. Mountain front sinuosity (S_{mf}) and river incision (V_f) points to active western and southern mountain fronts, and a northern inactive mountain front. These western and southern mountain fronts correspond with active NW–SE normal faults and E–W transfer strike-slip faults, respectively. On the contrary, the northern front corresponds with an inactive limb of an E–W antiformal ridge.

The asymmetry indexes calculated for the main catchments suggest the presence of active NNE–SSW oriented folds in the western part of the Sierra Nevada. These folds seem to be generated by isostatic adjustment related to the unroofing produced by the normal faults of the western Sierra Nevada mountain front (Martínez-Martínez et al., 2002).

The hypsometric curves and the longitudinal and ridge-line river profiles suggest a higher tectonic activity in the western part of the Sierra Nevada. Hypsometric curves also suggest, as well as S_{mf} and V_f, an inactive northern mountain front.

All the geomorphic indicators used in this work fit with the tectonic model proposed by Martínez-Martínez et al. (2006) for the

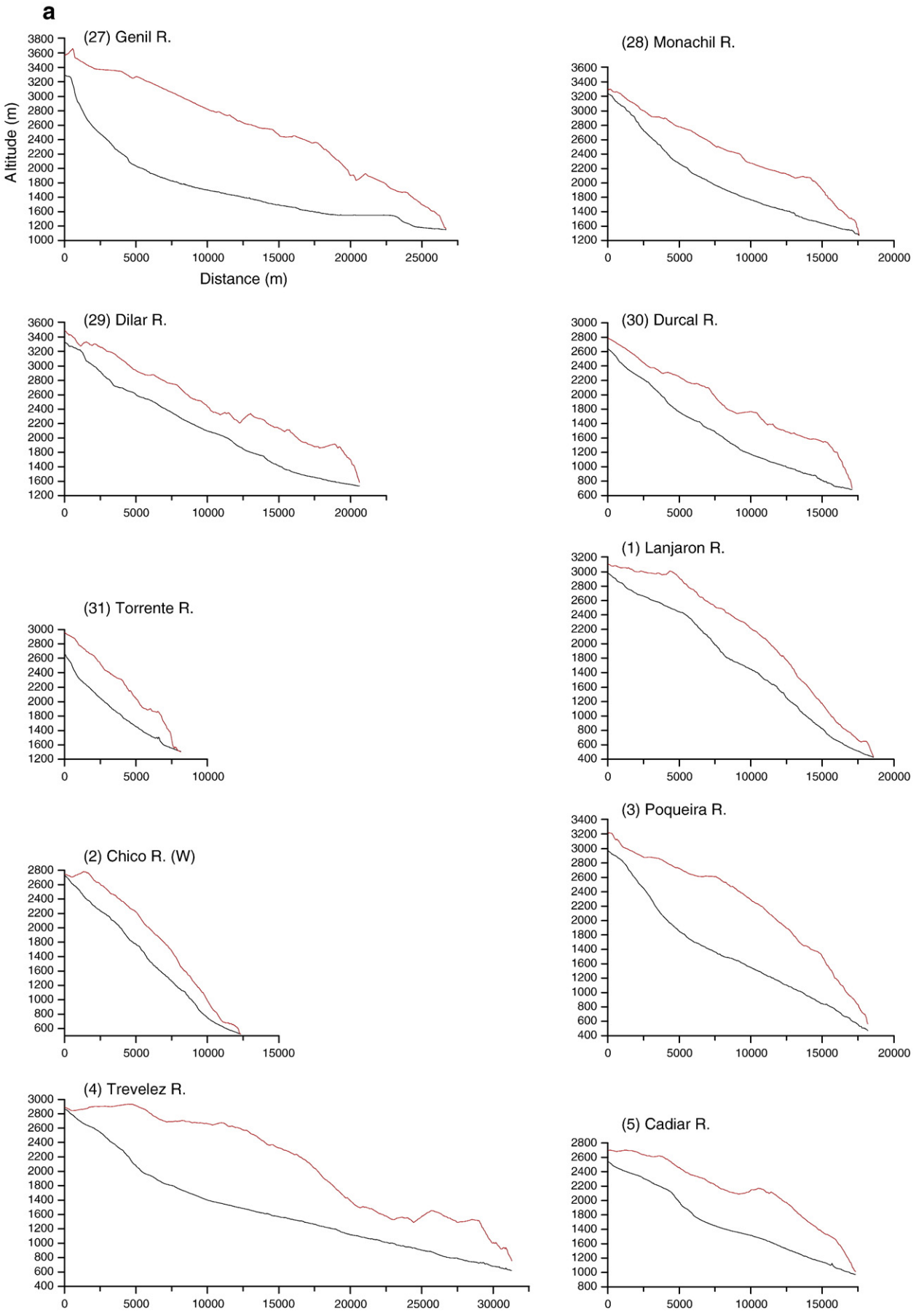
a
(27) Genil R.
(28) Monachil R.
(29) Dilar R.
(30) Durcal R.
(1) Lanjaron R.
(31) Torrente R.
(3) Poqueira R.
(2) Chico R. (W)
(4) Trevelez R.
(5) Cadiar R.
Altitude (m)
Distance (m)

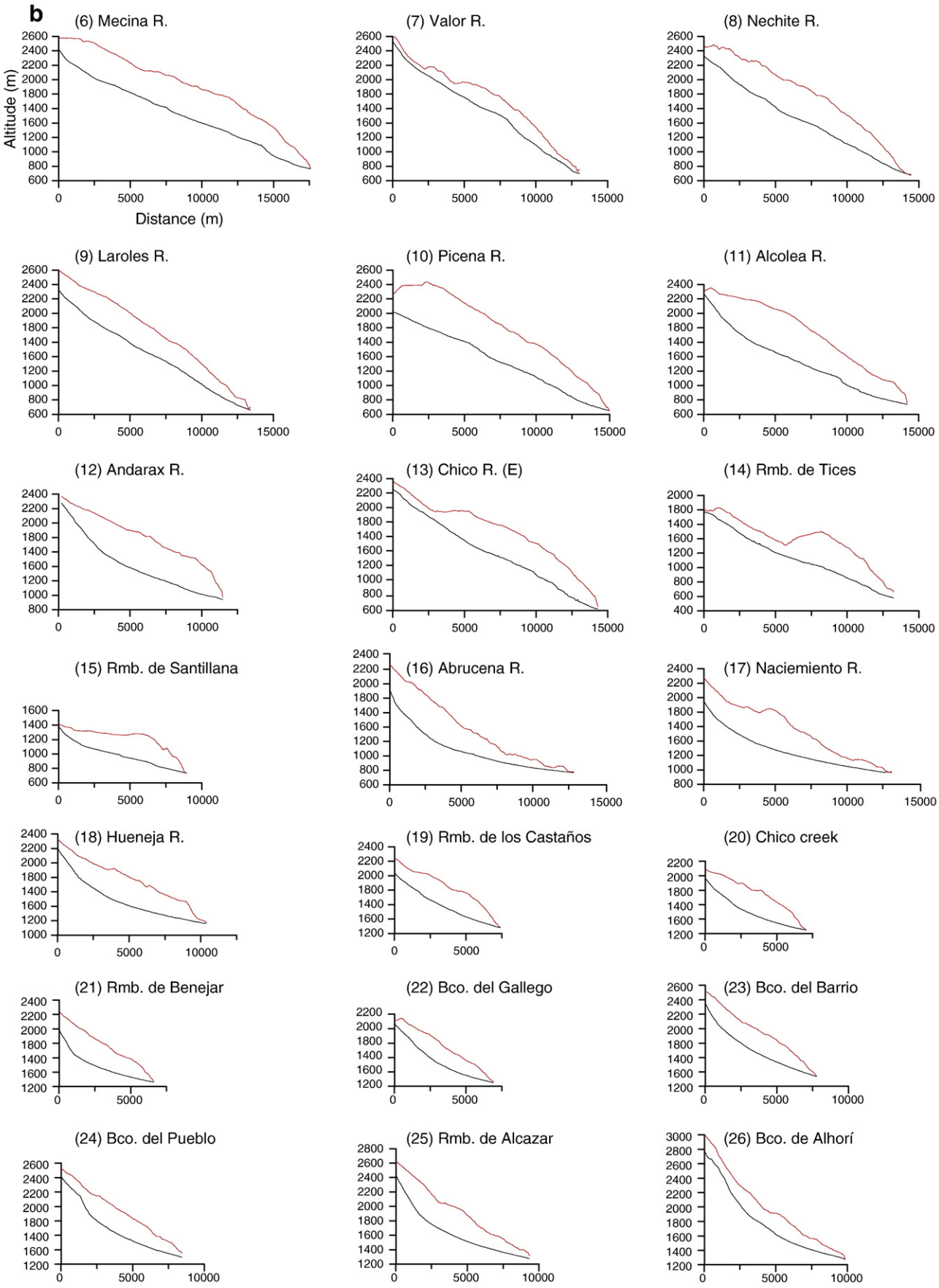

Fig. 8. Longitudinal and ridge-line profiles for the main rivers of the Sierra Nevada.

Sierra Nevada, with active western and southern fronts corresponding to normal and transfer strike-slip faults, respectively. This tectonic model also explains the topographic differences between the two neighboring Neogene–Quaternary basins (Granada and the Guadix–Baza basins). The Granada basin is located in the hanging wall of the SW-directed extensional system bounding the western the Sierra Nevada and, thus, is subjected to Quaternary subsidence. On the contrary, the Guadix–Baza basin is located in the footwall of the same system, being part, together with the whole Sierra Nevada, of a single block suffering tectonic uplift during the Quaternary.

Acknowledgements

This study was supported by the grants CGL2008-03249 and TOPO-IBERIA CONSOLIDER-INGENIO CSD2006-00041 of the Ministerio de Ciencia e Innovación, as well the project MMA 083/2007 of the Ministerio de Medio Ambiente y Medio Rural y Marino. We are thankful to Dr. Martínez-Martínez for his comments and suggestions on an early draft of this manuscript. We also thank Dr. Willian B. Bull and an anonymous referee for their constructive review comments.

References

Alfaro, P., Galindo-Zaldívar, J., Jabaloy Sánchez, A., López Garrido, A.C., Sanz de Galdeano, C., 2001. Evidence for the activity and paleoseismicity of the Padul fault (Betic Cordillera, SE Spain). Acta Geológica Hispánica 36, 283–295.

Azañón, J.M., Azor, A., Pérez-Peña, J.V., Carrillo, J.M., 2005. Late Quaternary large-scale rotational slides induced by river incision: the Arroyo de Gor area (Guadix basin, SE Spain). Geomorphology 69, 152–168.

Azor, A., Keller, E.A., Yeats, R.S., 2002. Geomorphic indicators of active fold growth: South Mountain-Oak Ridge anticline, Ventura basin, southern California. Geol. Soc. Am. Bull. 114, 745–753.

Balanyá, J.C., García-Dueñas, V., 1988. El Cabalgamiento cortical de Gibraltar y la tectónica de Béticas y Rif. II Congreso Geológico de España. Simposium sobre Cinturones Orogénicos.

Band, L.E., 1986. Topographic partition of watersheds with digital elevation models. Water Resour. Res. 22, 15–24.

Bishop, P., 2007. Long-term landscape evolution: linking tectonics and surface processes. Earth Surf. Proc. Land. 32, 329–365.

Braga, J.C., Martín, J.M., Quesada, C., 2003. Patterns and average rates of late Neogene–Recent uplift of the Betic Cordillera, SE Spain. Geomorphology 50, 3–26.

Brocklehurst, S.H., Whipple, K.X., 2002. Glacial erosion and relief production in the Eastern Sierra Nevada, California. Geomorphology 42, 1–24.

Bull, W.B., 1977. Tectonic geomorphology of the Mojave Desert, California. U.S. Geological Survey Contract Report 14-0-001-G-394. Office of Earthquakes, Volcanoes, and Engineering, Menlo Park, California. 188 pp.

Bull, W.B., 2007. Tectonic Geomorphology of Mountains: A New Approach to Paleoseismology. Wiley-Blackwell, Oxford. 328 pp.

Bull, W.B., 2009a. Tectonically Active Landscapes. Wiley-Blackwell, Oxford. 326 pp.

Bull, W.B., 2009b. Geomorphic Responses to Climatic Change. Blackburn Press, New Jersey. 326 pp.

Bull, W.B., McFadden, L.D., 1977. Tectonic geomorphology north and south of the Garlock fault, California. In: Doehering, D.O. (Ed.), Geomorphology in Arid Regions. Proceedings at the Eighth Annual Geomorphology Symposium. State University of New York, Binghamton, NY, pp. 115–138.

Burbank, D.W., Anderson, R.S., 2001. Tectonic Geomorphology. Blackwell Science, Oxford. 247 pp.

Calvache, M.L., Viseras, C., Fernández, J., 1997. Controls on fan development — evidence from fan morphometry and sedimentology; Sierra Nevada, SE Spain. Geomorphology 21, 69–84.

Clark, M.K., Schoenbohm, L.M., Royden, L.H., Whipple, K.X., Burchfiel, B.C., Zhang, X., Tang, W., Wang, E., Chen, L., 2004. Surface uplift, tectonics, and erosion of eastern Tibet from large-scale drainage patterns. Tectonics 23, TC1006.

Cloetingh, S., Cornu, T., 2005. Surveys on environmental tectonics. Quatern. Sci. Rev. 24, 235–240.

Comas, M.C., Platt, J.P., Soto, J.I., Watts, A.B., 1999. The origin and tectonic history of the Alboran basin: insights from Leg 161 results. In: Zahn, R., Comas, M.C., Klaus, A. (Eds.), Proc. ODP, Sci Results. Ocean Drilling Program, College Station, TX, pp. 555–579.

Cox, R.T., 1994. Analysis of drainage-basin symmetry as a rapid technique to identify areas of possible Quaternary tilt-block tectonics: an example from the Mississippi embayment. Geol. Soc. Am. Bull. 106, 571–581.

Davis, G.H., 1980. Structural characteristics of metamorphic core complexes, southern Arizona. In: Crittenden, M.D., Coney, P.J., Davis, G.H. (Eds.), Cordilleran Metamorphic Core Complexes, 153. Geological Society of America Memoir, pp. 35–77.

Davis, G.H., Constenius, K.N., Dickinson, W.R., Rodriguez, E.P., Cox, L.J., 2004. Fault and fault-rock characteristics associated with Cenozoic extension and core-complex evolution in the Catalina–Rincon region, southeastern Arizona. Geol. Soc. Am. Bull. 116, 128–141.

de Mets, C., Gordon, R.G., Argus, D.F., Stein, S., 1994. Effect of recent revisions to the geomagnetic reversal time-scale on estimates of current plate motions. Geophys. Res. Lett. 21, 2191–2194.

de Miguel, F., Vidal, F., Alguacil, G., Guirao, J.M., 1989. Spatial and energic trends of the microearthquakes activity in the Central Betics. Geodin. Acta 3, 87–94.

El Hamdouni, R., Irigaray, C., Fernández, T., Chacón, J., Keller, E.A., 2008. Assessment of relative active tectonics, southwest border of the Sierra Nevada (southern Spain). Geomorphology 96, 150–173.

England, P., Molnar, P., 1990. Surface uplift, uplift of rock, and exhumation of rocks. Geology 18, 1173–1177.

Galindo-Zaldívar, J., González Lodeiro, F., Jabaloy, A., 1989. Progressive extensional shear structures in a detachment contact in the Western Sierra Nevada (Betic Cordilleras, Spain). Geodin. Acta 3, 73–85.

Galindo-Zaldívar, J., Jabaloy, A., Serrano, I., Morales, J., González-Lodeiro, F., Torcal, F., 1999. Recent and present-day stresses in the Granada basin (Betic Cordilleras): example of a late Miocene-present-day extensional basin in a convergent plate boundary. Tectonics 18, 686–702.

Galindo-Zaldívar, J., Gil, A.J., Borque, M.J., González Lodeiro, F., Jabaloy Sánchez, A., Marín-Lechado, C., Ruano, P., Sanz de Galdeano, C., 2003. Active faulting in the internal zones of the central Betic Cordilleras (SE, Spain). J. of Geodynamics 36, 239–250.

García, A.F., Zhu, Z., Ku, T.L., Sanz de Galdeano, C., Chadwick, O.A., Montero, J.C., 2003. Tectonically driven landscape development within the eastern Alpujarran Corridor, Betic Cordillera, SE Spain (Almeria). Geomorphology 50, 83–110.

García-Dueñas, V., Balanyá, J.C., Martínez-Martínez, J.M., 1992. Miocene extensional detachments in the outcropping basement of the northern Alborán basin (Betics) and their tectonic implications. Geo-Mar. Lett. 12, 88–95.

Hancock, G.S., Anderson, R.S., 2002. Numerical modeling of fluvial strath-terrace formation in response to oscillating climate. Geol. Soc. Am. Bull. 114, 1131–1142.

Hare, P.W., Gardner, T.W., 1985. Geomorphic indicators of vertical neotectonism along converging plate margins, Nicoya Peninsula, Costa Rica. In: Morisawa, M., Hack, J.T. (Eds.), Tectonic Geomorphology. Proceedings of the 15th Annual Bighamton Geomorphology Symposium. Allen & Unwin, Boston, pp. 75–104.

Hetzel, R., Niedermann, S., Ivy-Ochs, S., Kubik, P.W., Tao, M.X., Gao, B., 2002. Ne-21 versus Be-10 and Al-26 exposure ages of fluvial terraces: the influence of crustal Ne in quartz. Earth Planet. Sci. Lett. 201, 575–591.

Hovius, N., 2000. Macroscale process systems of mountain belt erosion. In: Summerfield, M.A. (Ed.), Geomorphology and Global Tectonics. Wiley and Sons, Chichester, pp. 77–105.

Huang, X.J., Niemann, J.D., 2006. An evaluation of the geomorphically effective event for fluvial processes over long periods. J. of Geophys Res.–Earth Surf. 111, F03015.

Jackson, J., Van Dissen, R., Berryman, K., 1998. Tilting of active folds and faults in the Manawatu region, New Zealand: evidence from surface drainage patterns. NZ J. of Geol. Geophys. 41, 377–385.

Johnson, C., 1997. Resolving denudational histories in orogenic belts with apatite fission-track thermochronology and structural data: an example from southern Spain. Geology 25, 623–626.

Keller, E.A., 1986. Investigation of active tectonics: use of surficial earth processes. Active Tectonics National Academy Press, Washington D.C.

Keller, E.A., Pinter, N., 2002. Active Tectonics. Earthquakes, Uplift, and Landscape. Prentice Hall, New Jersey. 362 pp.

Keller, E.A., Sanz de Galdeano, C., Chacon, J., 1996. Tectonic geomorphology and earthquake hazard of Sierra Nevada, Southern Spain. 1ª Conferencia Internacional Sierra Nevada. Publicaciones Universidad de Granada, Granada, pp. 201–218.

Keller, E.A., Seaver, D.B., Laduzinsky, D.L., Johnson, D.L., Ku, T.L., 2000. Tectonic geomorphology of active folding over buried reverse faults: San Emigdio Mountain front, southern San Joaquin Valley, California. Geol. Soc. Am. Bull. 112, 86–97.

Lonergan, L., Platt, J.P., 1995. The Malaguide–Alpujarride boundary — a major extensional contact in the internal zone of the Eastern Betic Cordillera, SE Spain. J. Struct. Geol. 17, 1655–1671.

Martínez-Martínez, J.M., Soto, J.I., Balanyá, J.C., 1997. Crustal decoupling and intracrustal flow beneath domal exhumed core complexes, Betics (SE Spain). Terra Nova 9, 223–227.

Martínez-Martínez, J.M., Soto, J.I., Balanyá, J.C., 2002. Orthogonal folding of extensional detachments: structure and origin of the Sierra Nevada elongated dome (Betics, Spain). Tectonics 21, 1–22.

Martínez-Martínez, J.M., Soto, J.I., Balanyá, J.C., 2004. Elongated domes in extended orogens: a mode of mountain uplift in the Betics (southeast Spain). In: Whitney, D.L., Teyssier, C., Siddoway, C.S. (Eds.), Gneiss Domes in Orogeny. Geological Society of America, Boulder, Colorado, pp. 243–266.

Martínez-Martínez, J.M., Booth-Rea, G., Azañón, J.M., Torcal, F., 2006. Active transfer fault zone linking a segmented extensional system (Betics, southern Spain): insight into heterogeneous extension driven by edge delamination. Tectonophysics 422, 159–173.

Martín-Rojas, I., Martín-Martín, M., Sanz de Galdeano, C., 2001. Índices geomorfológicos de los frentes montañosos del borde occidental de Sierra Nevada (Granada — España). In: Pelaez Montilla, J., López Garrido, A.C. (Eds.), La Cuenca de Granada. In: Sanz de Galdeano, C. (Ed.), Estructura, Tectónica Activa, Sismicidad, Geomorfología y Dataciones Existentes. Universidad de Granada, Granada, pp. 59–66.

Menéndez, I., Silva, P.G., Martín-Betancor, M., Pérez-Torrado, F.J., Guillou, H., Scaillet, S., 2008. Fluvial dissection, isostatic uplift, and geomorphological evolution of volcanic islands (Gran Canaria, Canary Islands, Spain). Geomorphology 102, 189–203.

Moglen, G.E., Bras, R.L., 1995. The effect of spatial heterogeneities on geomorphic expression in a model of basin evolution. Water Resour. Res. 31, 2613–2623.

Molin, P., Pazzaglia, F.J., Dramis, F., 2004. Geomorphic expression of active tectonics in a rapidly-deforming forearc, Sila massif, Calabria, southern Italy. Am. J. Sci. 304, 559–589.
Morales, J., Serrano, I., Vidal, F., Torcal, F., 1997. The depth of the earthquake activity in the Central Betics (Southern Spain). Geophys. Res. Lett. 24, 3289–3292.
Morales, J., Serrano, I., Jabaloy Sánchez, A., Galindo-Zaldívar, J., Zhao, D., Torcal, F., Vidal, F., González-Lodeiro, F., 1999. Active continental subduction beneath the Betic Cordillera and the Alborán Sea. Geology 27, 735–738.
Muñoz, D., Cisternas, A., Udías, A., Mezcua, J., Sanz de Galdeano, C., Morales, J., Sánchez-Venero, M., Haessler, H., Ibáñez, J., Buforn, E., Pascual, G., Rivera, L., 2002. Microseismicity and tectonics in the Granada basin (Spain). Tectonophysics 356, 233–252.
Orozco, M., Alvarez-Valero, A.M., Alonso-Chaves, F.M., Platt, J.P., 2004. Internal structure of a collapsed terrain. The Lujar syncline and its significance for the fold- and sheet-structure of the Alboran domain (Betic Cordilleras, Spain). Tectonophysics 385, 85–104.
Pedrera, A., Pérez-Peña, J.V., Galindo-Zaldívar, J., Azañón, J.M., Azor, A., 2009. Testing the sensitivity of geomorphic indices in areas of low-rate active folding (eastern Betic Cordillera, Spain). Geomorphology 105, 218–231.
Pérez-Peña, J.V., Azañón, J.M., Azor, A., Tuccimei, P., Della Seta, M., Soligo, M., 2009a. Quaternary landscape evolution and erosion rates for an intramontane Neogene basin (Guadix–Baza basin, SE Spain). Geomorphology 106, 206–218.
Pérez-Peña, J.V., Azañón, J.M., Azor, A., 2009b. CalHypso: an ArcGIS extension to calculate hypsometric curves and their statistical moments. Applications to drainage basin analysis in SE Spain. Computers and Geosci. 35, 1214–1223.
Pérez-Peña, J.V., A., J.M., Azor, A., Delgado, J., González-Lodeiro, F., 2009c. Spatial analysis of stream power using GIS: SLk anomaly maps. Earth Surf. Proc. Land. 34, 16–25.
Pérez-Peña, J.V., Azañón, J.M., Booth-Rea, G., Azor, A., Delgado, J., 2009d. Differentiating geology and tectonics using a spatial autocorrelation 3 technique for the hypsometric integra. J. of Geophys. Res.–Earth Surf. 114, F02018.
Peuker, T.K., Douglas, D.H., 1975. Detection of surface-specific points by local parallel processing of discrete terrain elevation data. Comput. Graph. and Image Process. 4, 375–387.
Platt, J.P., Vissers, R.L.M., 1989. Extensional collapse of thickened continental lithosphere: a working hypothesis for the Alboran Sea and Gibraltar. Arc. Geol. 17, 540–543.
Reinhardt, L.J., Bishop, P., Hoey, T.B., Dempster, T.J., Sanderson, D.C.W., 2007. Quantification of the transient response to base-level fall in a small mountain catchment: Sierra Nevada, southern Spain. J. of Geophys. Res.-Earth Surf. 112, F03S05.
Ruano, P., 2003. Estructuras tectónicas recientes en la transversal central de las Cordilleras Béticas. Ph.D. Thesis, University of Granada, Granada.
Salvany, J.M., 2004. Tilting neotectonics of the Guadiamar drainage basin, SW Spain. Earth Surf. Proc. Land. 29, 145–160.
Sanz de Galdeano, C., 1976. Datos sobre las deformaciones neogenas y cuaternarias del sector del Padúl (Granada). Reunión Sobre la Geodinámica de las Cordilleras Béticas y el Mar de Alborán. Univ. Granada, Granada, pp. 197–218.
Sanz de Galdeano, C., 1985. La fracturación del borde sur de la depresión de Granada (Discusión acerca del escenario del terremoto del 25-XII-1884). Estud. Geol. 41, 59–68.
Sanz de Galdeano, C., 1996. Datos sobre las deformaciones neógenas y cuaternarias del sector del Padul (Granada). 1ª Conferencia Internacional Sierra Nevada. Publicaciones Universidad de Granada, Granada, pp. 219–231.
Sanz de Galdeano, C., Alfaro, P., 2004. Tectonic significance of the present relief of the Betic Cordillera. Geomorphology 63, 175–190.
Sanz de Galdeano, C., López-Garrido, A.C., 1999. Nature and impact of the Neotectonic deformation in the western Sierra Nevada (Spain). Geomorphology 30, 259–272.
Sanz de Galdeano, C., Rodríguez-Fernández, J., 1985. A strike-slip-fault corridor within the Alpujarra Mountains (Betic-Cordilleras, Spain). Geol. Rundsch. 74, 641–655.
Schoenbohm, L.M., Whipple, K.X., Burchfiel, B.C., Chen, L., 2004. Geomorphic constraints on surface uplift, exhumation, and plateau growth in the Red River region, Yunnan Province, China. Geol. Soc. Am. Bull. 116, 895–909.
Schumm, S.A., Dumont, J.F., Holbrook, J.M., 2000. Active Tectonics and Alluvial Rivers. Cambridge University Press, Cambridge. 276 pp.
Silva, P.G., Goy, J.L., Zazo, C., Bardají, T., 2003. Fault-generated mountain fronts in southeast Spain: geomorphologic assessment of tectonic and seismic activity. Geomorphology 50, 203–225.
Soria, J.M., Viseras, C., Fernández, J., 1998. Late Miocene–Pleistocene tectono-sedimentary evolution and subsidence history of the central Betic Cordillera (Spain): a case study in the Guadix intramontane basin. Geol. Mag. 135, 565–574.
Starkel, L., 2003. Climatically controlled terraces in uplifting mountain areas. Quatern. Sci. Rev. 22, 2189–2198.
Strahler, A.N., 1952. Hypsometric (area-altitude) analysis of erosional topography. Geol. Soc. Am. Bull. 63, 1117–1142.
Tarboton, D.G., 1997. A new method for the determination of flow directions and upslope areas in grid digital elevation models. Water Resour. Res. 33, 309–319.
Viseras, C., Calvache, M.L., Soria, J.M., Fernández, J., 2003. Differential features of alluvial fans controlled by tectonic or eustatic accommodation space. Examples from the Betic Cordillera, Spain. Geomorphology 50, 181–202.
Walcott, R.C., Summerfield, M.A., 2008. Scale dependence of hypsometric integrals: an analysis of southeast African basins. Geomorphology 96, 174–186.
Watchman, A.L., Twidale, C.R., 2002. Relative and 'absolute' dating of land surfaces. Earth-Sci. Rev. 58, 1–49.
Watts, A.B., Platt, J.P., Bulh, P., 1993. Tectonic evolution of the Alboran Sea basin. Basin Res. 5, 153–177.
Willgoose, G., Hancock, G., 1998. Revisiting the hypsometric curve as an indicator of form and process in transport-limited catchment. Earth Surf. Proc. Land. 23, 611–623.